Environ. Sci. Technol. **2007**, *41,* 5738−5746

Disentangling Oil Weathering Using GC×GC. 1. Chromatogram Analysis

J. SAMUEL AREY,[†]
ROBERT K. NELSON,[‡] AND
CHRISTOPHER M. REDDY[‡]

Laboratory of Biochemistry and Computational Chemistry, Swiss Federal Institute of Technology, Lausanne, Switzerland, and Department of Marine Chemistry and Geochemistry, Woods Hole Oceanographic Institution, Woods Hole, Massachusetts

Historically, the thousands of compounds found in oils constituted an "unresolved complex mixture" that frustrated efforts to analyze oil weathering. Moreover, different weathering processes inflict rich and diverse signatures of compositional change in oil, and conventional methods do not effectively decode this elaborate record. Using comprehensive two-dimensional gas chromatography (GC×GC), we can separate thousands of hydrocarbon components and simultaneously estimate their chemical properties. We investigated 13 weathered field samples collected from the *Bouchard 120* heavy fuel oil spill in Buzzards Bay, Massachusetts in 2003. We first mapped hydrocarbon vapor pressures and aqueous solubilities onto the compositional space explored by GC×GC chromatograms of weathered samples. Then we developed methods to quantitatively decouple mass loss patterns associated with evaporation and dissolution. The compositional complexity of oil, traditionally considered an obstacle, was now an advantage. We exploited the large inventory of chemical information encoded in oil to robustly differentiate signatures of mass transfer to air and water. With this new approach, we can evaluate mass transfer models (the Part 2 companion to this paper) and more properly account for evaporation, dissolution, and degradation of oil in the environment.

Introduction

About 750 million liters of crude and refined petroleum enter the sea annually from anthropogenic sources, and natural ocean floor seeps contribute a similar amount (*1*). In the environment, the petroleum mixture weathers via processes that span hours to decades. Evaporation, dissolution, and sorption preferentially transfer some chemical components out of the mixture (*2*−*5*). Microbial degradation and photodegradation transform certain compounds (*3*, *6*−*8*). These natural removal processes are chemically selective, and their rates influence the duration and extent of damage to coastal ecosystems (*1*). Mass transfers of hydrocarbon compounds to different environmental compartments (water, air, sediments, biota) partly control biotic exposures (*1*, *9*). For example, hydrocarbon concentrations in the water column are used to estimate injuries to aquatic wildlife (*9*−*11*), and this informs court settlement and environmental restoration decisions under the U.S. Oil Pollution Act of 1990 (33 USC 2701−2761). Scientists have studied oil weathering for over three decades, and nonetheless the underlying processes are still difficult to decouple and quantify for most hydrocarbon compounds.

Commonly, investigators diagnose weathering by comparing concentration ratios of carefully chosen compound sets between differently weathered oils (*12*). However this data analysis technique may not robustly differentiate some weathering processes. The driving assumption is that one compound set (e.g., the denominator) is consistently more responsive to weathering than the other compound set (numerator). This enables a quantitative characterization that can be compared across different oil samples. From our literature search, over a dozen concentration ratios have been proposed to indicate weathering (Table 1). Compound ratios can more confidently diagnose biodegradation than evaporation or dissolution. For example, structural isomers of a given hydrocarbon compound have similar partitioning properties (*5*) but often have different susceptibilities to biodegradation (*12*). Consequently, compound ratios of structural isomers can unequivocally diagnose a chemical transformation process, independent of evaporation and dissolution effects. However, it is more difficult to find sets of compound structures that biodegrade at the same rate and that also vary across the relevant span of volatility or aqueous solubility. Therefore it is difficult to devise ratios that interrogate evaporation or dissolution. Finally, the diagnosis attributed to a given ratio is sometimes inconsistent between studies. For example, polycyclic aromatic hydrocarbon (PAH) weathering rate often decreases with increasing PAH size and increasing alkyl substitution, but this pattern has been attributed to both biodegradation (*7*, *13*) and dissolution (*14*, *15*). Properly differentiating these processes requires detailed accounting of many compounds having diverse reactivities and chemical properties.

Conventionally, one-dimensional gas chromatography (GC) is employed to probe the evolution of oil composition during weathering (*12*). Gas chromatography−mass spectrometry (GC−MS) enables identification and quantification of hundreds of hydrocarbons (*16*, *17*). By comparison, comprehensive two-dimensional gas chromatography (GC×GC) is a young technology (*18*) that separates thousands of peaks in oils and extracts; it has mostly resolved the previously "unresolved complex mixture" in weathered oils (*19*) and mussel tissues (*20*). GC×GC−FID (flame ionization detection) offers some advantages over GC−MS, including improved separation and lower variability in response factor between compounds (*19*, *21*).

Recent work suggests that GC×GC could be used to analyze compositional changes due to evaporation and dissolution. Arey et al. (*22*, *23*) developed a method for estimating the two GC×GC retention indices, I_1 and I_2, of hydrocarbon solutes. This basis contains enough information to estimate several environmental partitioning properties for hydrocarbons, via

$$\log P_i = aI_{i,1} + bI_{i,2} + c \qquad (1)$$

where P_i is a partitioning property of solute i, and a, b, and c are fitted coefficients that depend on the partitioning property. Thus vapor pressure and aqueous solubility estimates for hydrocarbon compounds can be directly mapped onto the complete GC×GC chromatogram of a realistic diesel-range oil mixture (*22*).

* Corresponding author phone: +41 21 693 0322; fax: +41 21 693 0320; e-mail: arey@alum.mit.edu.
[†] Swiss Federal Institute of Technology.
[‡] Woods Hole Oceanographic Institution.

10.1021/es070005x CCC: $37.00

Published on Web 07/14/2007

TABLE 1. Chemical Ratios Commonly Used to Diagnose Oil Weathering (Due to Space Constraints, the Reference List Is Not Comprehensive)[a]

chemical ratio	diagnosed process	references
$(\sum C_8-C_{14})/(\sum C_{22}-C_{28})$	evaporation	*16, 36, 37*
$(\sum C_{10}-C_{25})/(\sum C_{17}-C_{25})$	evaporation	*14*
isoprenoid$_n$/pristane, for $n = 13$ to 16	evaporation	*38*
$\sum (N + F + P + D)/\sum (P + D)$	evaporation, dissolution	*14*
relative distribution of alkyl-substituted PAHs	dissolution	*15*
$(C_{12}-C_{18})$/(equivalent weight isoprenoid)	biodegradation	*3, 14, 37−44*
relative distribution of alkyl substituted PAHs	biodegradation	*45*
($\sum$ odd *n*-alkanes)/($\sum$ even *n*-alkanes)	biodegradation	*37*
$(1,3\text{-}C_2N + 1,6\text{-}C_2N)/\sum C_2N$	biodegradation	*37, 39*
"methyl-F"/$\sum C_1F$	biodegradation	*37, 39*
$(2\text{-}C_1D$ or $3\text{-}C_1D)/4\text{-}C_1D$	biodegradation	*39, 44*
various ratios of C_1D isomers	biodegradation	*37, 40*
A/P and BAP/BEP	photodegradation	*46*
relative distribution of alkyl substituted PAHs	photodegradation	*8*
C_2D/C_2P and C_3D/C_3P	general weathering	*13, 15, 47*
F/C_1P and C_3N/C_2P and D/C_4P	general weathering	*13*
$(C_2D$ or $C_2P)/C_2C$ and $(C_3D$ or $C_3P)/C_3Ch$	general weathering	*13, 15, 43, 48*
$\sum$ Ch/($\sum$ N or $\sum$ D or $\sum$ P or $\sum$ F)	general weathering	*34, 36, 37, 40, 47*
relative distribution of alkyl substituted PAHs	general weathering	*34, 36, 37, 39, 40, 49, 50*
($\sum$ N or $\sum$ P)/$\sum$ PAH	general weathering	*15, 43, 51*

[a] Abbreviations: C_i, *n*-alkane or alkyl substituent of chain length *j*; PAH, polycyclic aromatic hydrocarbon; N, naphthalene; F, fluorene; D, dibenzothiophene; P, phenanthrene; A, anthracene; Ch, chrysene; BAP, benzo[*a*]pyrene; BEP, benzo[*e*]pyrene.

In this study, we aimed to diagnose the effects of evaporation and dissolution on the oil mixture compositions of real weathered samples. We hypothesized that by projecting physical properties onto observed changes in oil composition in GC×GC chromatograms, we could differentiate evaporation and dissolution from other weathering effects. In this way, we interrogated weathering processes based on the behaviors of thousands of compounds in the oil, rather than just a few compound ratios. To test the hypothesis, we evaluated oil samples obtained from a heavily contaminated cobble beach (Nyes Neck beach on Buzzards Bay, MA) during the first 16 weeks after the *Bouchard 120* fuel oil spill of 2003. In a companion paper (part 2), we extend this analysis and apply a detailed mass transfer model of evaporation and dissolution to this same site (*24*).

Materials and Methods

Sample Collection and Preparation. Sample collection and preparation methods were detailed in previous work (*25*). Briefly, oil-covered rocks (2−4 cm diameter) were collected from Nyes Neck beach in North Falmouth, MA, during a 4 month period (May 6−Aug 18) after the *Bouchard 120* spill (April 27). Small cobbles were collected from the "surf zone", which was regularly exposed to both wind and water, and also from the high beach ("dry zone"). A neap tide, concurrent with the spill, deposited some oil unusually far into the high beach, hence waves rarely reached the dry zone. To evaluate inter-sample variability, our sample set included three separate cobbles from the same day and zone (surf zone, day 86, "A, B, C"). In the field, each sample was transferred to a sealed glass jar with ~40 mL of dichloromethane/methanol (90:10). Samples were then solvent extracted with dichloromethane/methanol and solvent exchanged into hexane to remove asphaltenes. Thirteen of these extracts, plus the original *Bouchard 120* heavy oil, were analyzed using GC×GC.

GC×GC Analysis. Each sample extract was analyzed using GC×GC−FID. In GC×GC, a sample mixture is separated using two columns that are joined serially by a cryogenic modulator. Mixture components eluting from the first "dimension" (a nonpolar column) are trapped by the modulator and then fully transferred to the second dimension (a semipolar column) at discrete time intervals. The first and second dimension columns were housed in separate ovens having independent temperature programs. The temperature program is fully described in "GC×GC Method A" and the column characteristics correspond to "GC×GC Method B" of our previous work (*22*).

Data Analysis

Chromatogram Preparation and Physical−Chemical Property Analysis. Each raw GC×GC chromatogram was preprocessed to facilitate meaningful quantitative analysis and mass comparisons between samples. First, the chromatogram baseline was removed (*26*). Second, all pixels having FID response height <0.1 pA were considered noise and were set to zero. All FID response information that eluted earlier than 0.15 s before *n*-alkanes in the second dimension was considered artifactual (i.e., modulated column bleed) and set to zero peak height. Finally, solvent bleed interfered with peaks eluting before C_{11}, and this material, which we estimate comprised <3% of the original oil mass, was excluded from analysis.

Individual peak volumes of major peaks (e.g., *n*-alkanes) were calculated using an automated peak integration tool (*27*). For best precision, volumes of the $C_{30}-C_{35}$ hopane peaks were integrated using a customized algorithm developed in our lab (see Supporting Information). All chromatograms were normalized to C_{30} 17α,21β(H)-hopane, a compound often assumed conserved during weathering (*28*).

Mapping Hydrocarbon Partitioning Properties onto GC×GC Chromatograms. Using eq 1, estimates of the (hypothetical pure liquid) vapor pressures and aqueous solubilities were projected onto each GC×GC chromatogram (*22*), assuming that these peaks represented hydrocarbon compounds. Raoult's law applies to hydrocarbon compounds in oil mixtures (*29*), hence these pure liquid properties were used to estimate the oil−air partition coefficients and oil−water partition coefficients of hydrocarbons across the GC×GC chromatogram (*24*). It was desirable to map estimates of solute molecular weight onto the GC×GC chromatogram. For example, molecular weight information allows solute diffusivity estimates in gas and liquid phases (*5*). The GC×GC two-dimensional retention index conveys information about both the size and saturation of analyzed hydrocarbon solutes (*22*). We surmised that this reflected sufficient information to estimate molecular weights of hydrocarbon solutes. Using

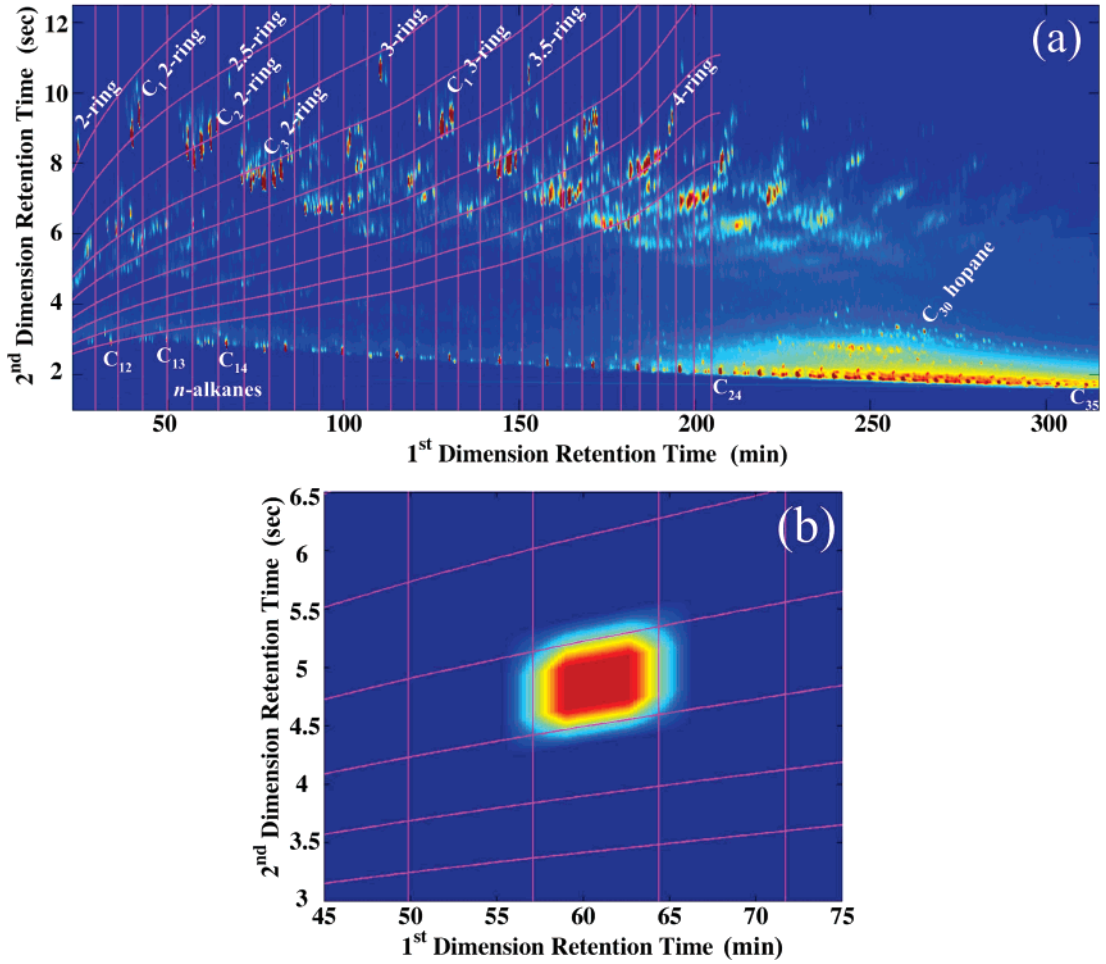

FIGURE 1. Chemical property contour map of a GC×GC chromatogram. (a) A GC × GC chromatogram of *Bouchard 120* oil. Solute vapor pressure and aqueous solubility were mapped onto the compositional space of compounds eluting in the *n*-alkane C_{11}−C_{24} boiling range (*22*). Solute vapor pressure contours (pink vertical lines) decrease from left to right along the first dimension retention time. Solute aqueous solubility contours (pink curved lines) decrease from upper left to lower right. (b) The weighting function for a single finite element cell is depicted as a heat map, overlaid on the vapor pressure and aqueous solubility contours. The weighting function equals zero far away from cell boundaries (dark blue); it is linearly sloped near cell boundaries so as to intercept cell boundaries at a value of 0.5 (light blue); and it attains a value of 1.0 (red) at 1/4 of the cell length from the boundary. Assignment of chromatogram mass into individual finite element cells was defined by this weighting function across the entire chromatogram.

the two-dimensional retention index developed by Arey et al. (*22*) for the 57 hydrocarbon solutes studied in that work, we found

$$\mathrm{mw}_i = 0.296I_{i,1} - 0.169I_{i,2} + 26.7 \quad r^2 = 0.988 \quad \mathrm{SD} = 6.0\ \mathrm{Da} \quad (2)$$

by multiple linear regression. The coefficients of eq 2 depend slightly on the particular settings of the GC×GC setup and temperature program (*22*).

Two-Dimensional Finite Element Discretization of GC×GC Chromatograms. To accomplish the physical weathering analysis, we discretized the GC×GC chromatogram into a low-resolution, two-dimensional grid of cells. Finite element cell boundaries were defined by contours of hydrocarbon vapor pressure and aqueous solubility (Figure 1a), such that each cell had dimensions of 0.2 in log vapor pressure and 0.5 in log solubility. Chromatogram peaks sharing a given cell therefore have similar physical properties. "Cell mass" was defined as the sum of all pixel heights assigned to a cell. During method development, we found that some chromatogram peaks inevitably lie across discrete cell boundaries, so that small shifts in peak retention time at a cell boundary would cause spurious changes in cell mass. To robustly compare cell masses between different sample chromatograms, the cell masses must be insensitive to these slight peak shifts. Thus the chromatogram pixels near a cell boundary were partly assigned to the cells at both sides of the boundary, according to overlapping trapezoidal weighting functions (Figure 1b). The resulting finite element discretization is mass-conserving: the total chromatogram sum of pixel masses (in the C_{11} to C_{24} range) is equal to the sum of the finite element cell masses. Note that since the discretization is two-dimensional, a chromatogram pixel near the intersection of two finite element boundaries may be assigned to as many as four cells (Figure 1b).

Results and Discussion

GC×GC Chemical Property Maps. A contour map of vapor pressure and aqueous solubility was overlaid onto the raw GC×GC chromatogram of the *Bouchard 120* cargo hold oil (Figure 1a). We expected hydrocarbon volatility and solubility to control evaporation and dissolution rates, respectively (*24*). The chemical property estimates have been validated for the compositional space corresponding to the C_{10}−C_{24} boiling range (*22*) and not for larger compounds. This boiling range includes, for example, the two-ring through four-ring parent PAHs. This compositional space was considered adequate for analyzing early evaporation and dissolution kinetics. Additionally, the aqueous solubility estimates of saturated

hydrocarbons having chain length $>C_{11}$ are only semiquantitative (*22*). This was considered unlikely to limit our analyses, since dissolution of large *n*-alkanes would require very severe water-washing circumstances. Under realistic conditions, evaporation or biodegradation would remove these saturates long before dissolution.

Discerning Evaporation and Dissolution Signatures using Mass Loss Tables (MLTs). Comparisons between weathered samples and fresh *Bouchard 120* oil elucidated the coverage and magnitude of mass transfer signatures across the GC×GC chromatograms (Figure 2). We expected evaporation to systematically remove compounds along the first dimension of the chromatogram, corresponding to increasing hydrocarbon boiling point (Figure 2c). Likewise, dissolution should remove compounds along a path perpendicular to solubility contours (Figure 2c), initially removing small aromatic compounds (most soluble). Using finite element cells defined by intersecting contours of vapor pressure and aqueous solubility (Figure 1), we compared weathering trends between samples. For each cell *i*, we evaluated the ln-transformed fraction of mass remaining, $\ln [M_i(t)/M_i(t_0)]$, of the weathered samples (time *t*) with respect to the fresh oil (time t_0). Each weathered oil chromatogram was thus transformed into an array of cells depicting compositional changes along systematic coordinates of volatility and aqueous solubility. We named this array a "mass loss table" or MLT (Figure 2d). The black shaded regions of the MLT simply indicate that no compounds in the original oil occupied this part of the chemical property space. Inspection of MLTs enabled quantitative inferences about evaporation and dissolution effects.

At Nyes Neck beach, a strong evaporation signature was evident in all spring and summer samples (May 6−August 18, i.e., day 10−day 114). Samples collected from the surf zone were compared to samples collected from a higher, dry beach zone, only ~10 m away. Surf zone samples had been alternately exposed to the atmosphere and ocean water during every tidal cycle, whereas the higher beach samples experienced drier and warmer conditions (*24*). For all samples, the MLT rows exhibited a strong trend of mass loss with increasing hydrocarbon volatility (Figure 3). Additionally, for any given sample, several MLT rows exhibited steep gradients that clustered together around a characteristic vapor pressure range. This collective profile of mass loss gradients was identified as an evaporation "front": that is, a region that delineates a systematic progression of mass removal along the dimension of vapor pressure. In the earliest dry zone sample (day 16), initial atmospheric exposure positioned the evaporation front at approximately the 0.7 Pa vapor pressure contour (Figure 3b). The evaporation front progressed unambiguously across the volatility contours of the dry zone samples systematically with increased weathering time, eventually reaching components of <0.01 Pa vapor pressure by days 86 and 114 (Figure 3h and l). Air temperatures and solar exposure increased steadily throughout the course of the sampling period (*24*), consistent with the observed rapid advance of the evaporation front in dry zone samples. In the surf zone, evaporation exhibited a slower progression through the sample set. Except for the latest sample, all surf zone samples displayed an evaporation front at vapor pressures ranging from only 0.3 to 1.0 Pa. This suggests that in the surf zone, oil evaporation decelerated dramatically after the initial two weeks, compared to the dry zone. This difference is probably explained by the limited atmospheric exposure and decreased temperatures of the surf zone relative to the dry zone (*24*). Evaporation fronts of surf zone samples were also more erratic with time. For example, the day 86B surf zone sample (Figure 3j) displayed an evaporation front that was comparable to the day 10 surf zone sample (Figure 3a). Moreover, the 3 day 86 surf zone samples (A, B, C) exhibited variability in the evaporation front position of about a factor of 10 in the vapor pressure. This reflects the fact that different samples experienced unique physical weathering trajectories, due to differences in oil loading and varying exposure to air and water (*24*). Finally, in some samples, a small amount of highly volatile material appeared to persist in the left-most regions of the MLTs (Figure 2d). These peaks are probably analysis artifacts: they were observed in a blank run of pure solvent, suggesting that they derived from GC×GC column bleed or solvent impurities.

Note that hydrocarbon evaporation signatures might also be quantitatively estimated by inspection of a conventional, one-dimensional GC chromatogram. This is possible because hydrocarbon retention time on a nonpolar GC stationary phase accurately predicts volatility from an oil mixture (*22*, *30*). Reddy et al. (*31*) showed that evaporation systematically removes oil components along the first dimension retention time of a GC×GC chromatogram, consistent with the expectation (*22*) that the GC×GC second dimension does not confer additional information about hydrocarbon volatilization from the mixture. Hence, laboratories that do not use GC×GC could evaluate evaporative losses using conventional GC. Nonetheless, such analyses should be interpreted cautiously: both biodegradation (*7*) and dissolution also favor removal of small compounds, therefore either of these removal patterns may partly correlate with hydrocarbon volatility for a given mixture.

Dissolution signatures were elucidated from the sample set, with the surf zone displaying stronger signals than the dry zone (Figure 3). Any of the samples could be expected to show some dissolution evidence due to the brief water exposure of the *Bouchard 120* floating oil slick immediately after the spill. However, we anticipated that surf zone samples would display a stronger dissolution signal on average. The earliest samples showed only ambiguous evidence of a dissolution front (days 10−16, Figure 3a−c), suggesting that evaporation dominated mass removal during the first two weeks. The day 33 surf zone sample showed a more distinct dissolution front near the MLT solubility contour of $10^{-4.5}$ mol/L, and this signal was less pronounced in the day 33 dry zone sample. The day 60 surf zone sample also exhibited a dissolution front at the $10^{-4.5}$ mol/L solubility contour, but the corresponding MLT columns in the day 60 dry zone sample have been eliminated by evaporation. So we cannot compare the dissolution signature of the two samples from day 60. All 3 day 86 surf zone samples show strong dissolution signals in the $10^{-4.5}$ to $10^{-5.0}$ mol/L solubility range. Finally, the day 114 surf zone sample suggested a very advanced dissolution front in the $10^{-6.0}$ to $10^{-6.5}$ mol/L solubility range, although biodegradation or photodegradation of PAHs also could have contributed to this pattern. To more confidently distinguish dissolution losses from transformation processes, the mass loss patterns observed here were separately evaluated using mass transfer calculations (*24*).

Biodegradation, Photodegradation, and Other Processes Causing Compositional Change. In some samples, the C_{21}−C_{29} boiling range hydrocarbons showed an apparent slight mass gain relative to the original oil after normalization by the internal marker, C_{30} hopane. Notably, the samples that displayed this feature (day 10 surf zone, day 86 surf zone A−C) had been analyzed immediately after some small modifications to the GC×GC column plumbing. In these samples, trends suggested a small leak between the second dimension column and the FID. Carrier gas pressure was ramped continually through the run, and the increased pressure near the end of the run would exacerbate a minor leak at this connection. A small artifactual mass loss of late elutants (i.e., high boiling point compounds) would result. Hence, after normalizing by C_{30} hopane, the lower boiling

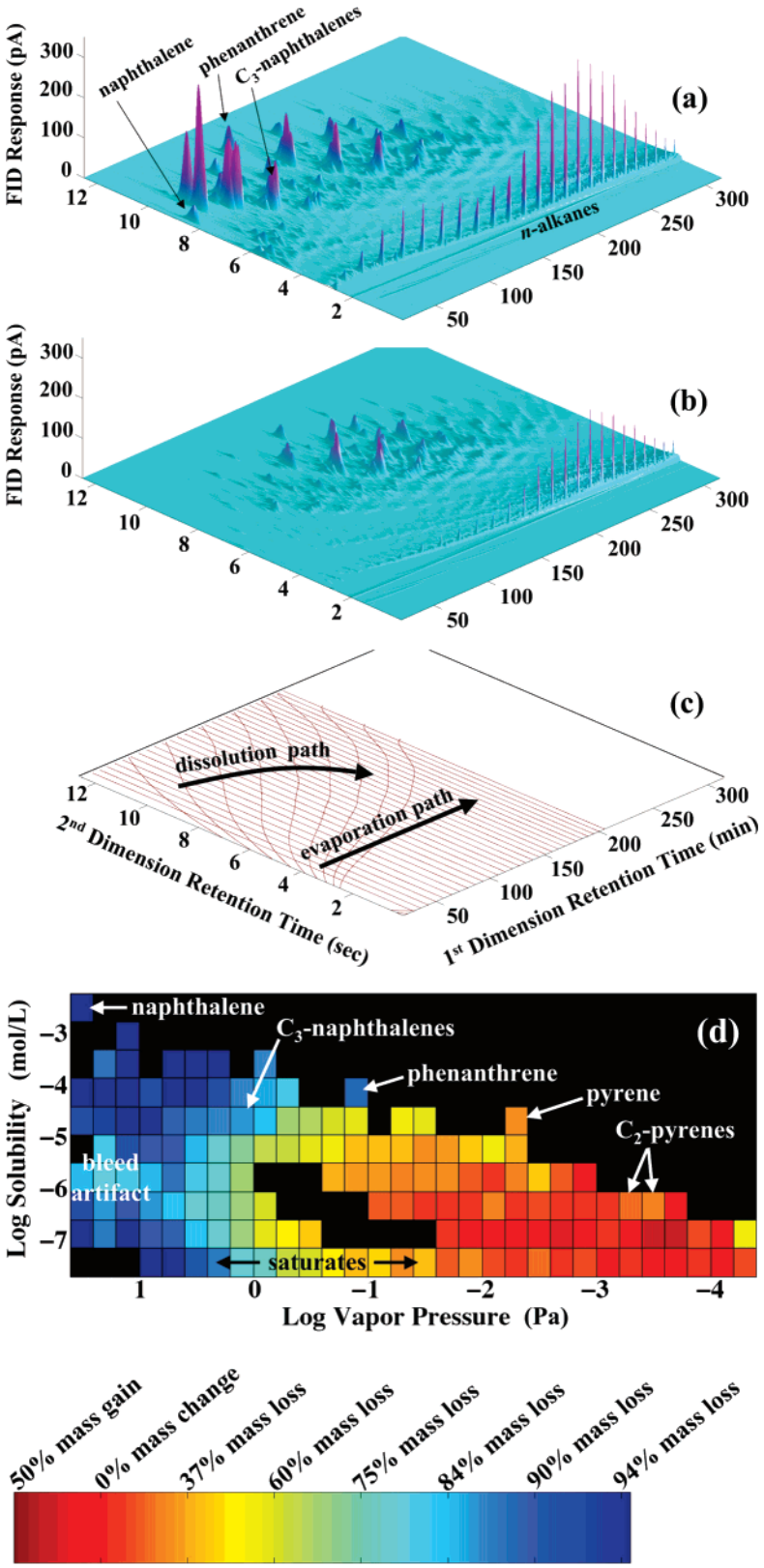

FIGURE 2. Conversion of a GC×GC chromatogram into a Mass Loss Table (MLT). (a) Mountain plot of the complete GC×GC chromatogram of original *Bouchard 120* oil. Because GC×GC−FID has similar response factors for different hydrocarbons, mountain plots accurately convey the relative mass abundances of different compounds. (b) Mountain plot of the day 60 surf zone sample. (c) Contours of hydrocarbon vapor pressure (straight lines) overlaid with contours of hydrocarbon aqueous solubility (curved lines). Evaporation and dissolution were expected to remove hydrocarbon mass along a path that is perpendicular to the corresponding partitioning property contour lines, as shown by the bold arrows. Finite element cells were delimited by these contours and their intersections. (d) The day 60 surf zone MLT, created by calculating the mass ratios of finite element cells in this sample with respect to corresponding cells in the original oil. Cells containing negligible peak information (defined as those having fewer than 400 pixels of height greater than 0.5 pA) were removed from the analysis; these cells are shaded black in the MLT. Some cells in the leftmost region contained a small amount of material from a column bleed artifact, as discussed in the text.

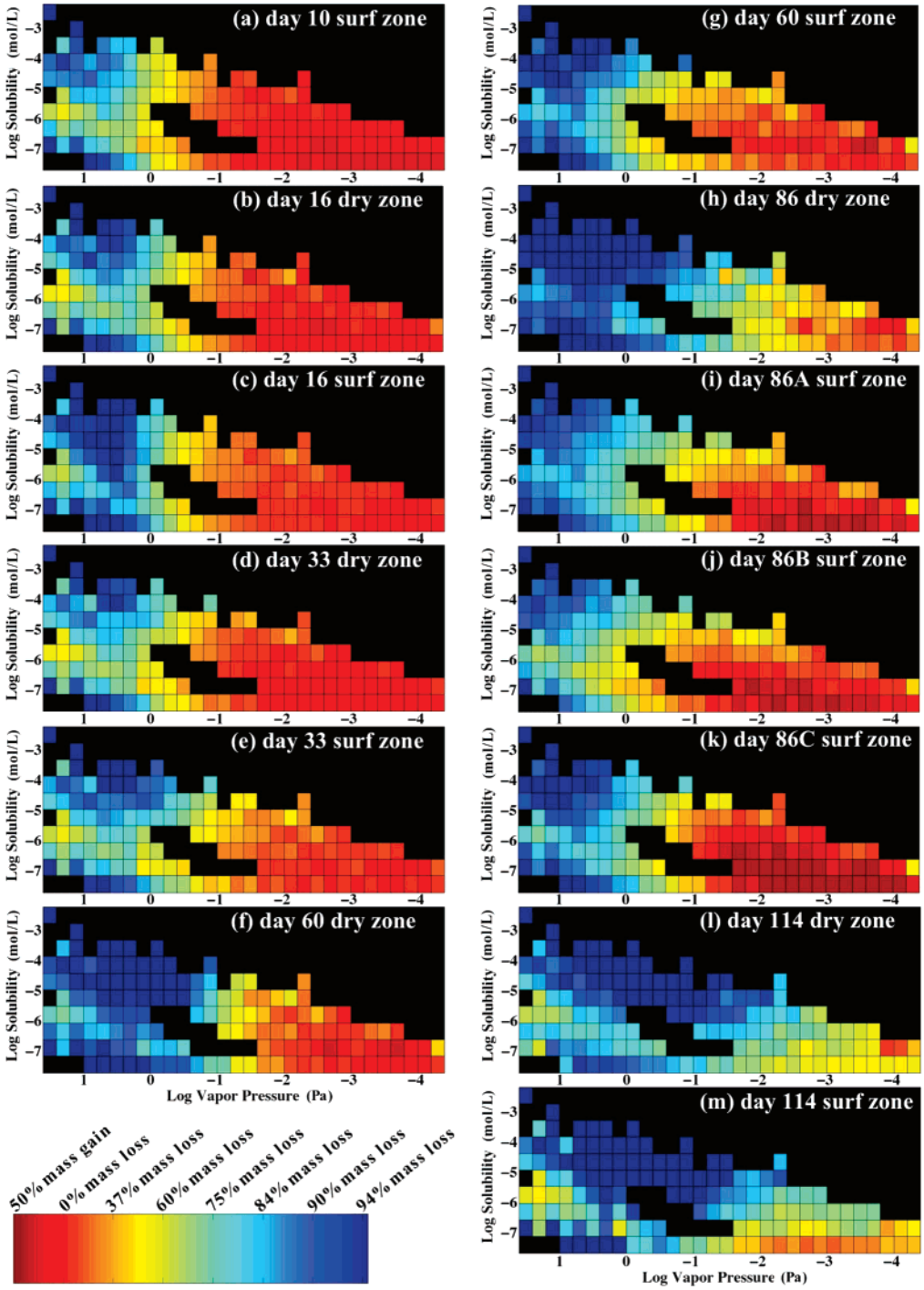

FIGURE 3. Mass Loss Tables (MLTs) of samples collected during the first 114 days of *Bouchard 120* weathering. MLTs depict compositional changes of weathered samples relative to the original *Bouchard 120* oil; mass changes are distributed orthogonally in the dimensions of volatility and solubility. Consequently every MLT row contains information that is tailored to diagnosing an evaporation signature without interference from possible dissolution effects. Likewise, every MLT column can be used to search for dissolution evidence independently of evaporation effects. As a result, an evaporation or dissolution signature was identified as a "front": a strong gradient of mass loss aligned with either vapor pressure or aqueous solubility. Some samples exhibited superimposed signatures of both evaporation and dissolution.

range elutants would appear inflated relative to the original reference oil. No attempt was made to correct the data for this artifact, which caused an estimated 10−40% distortion in the apparent mass abundances of lower boiling range compounds in affected samples. The empirical evaporation fronts examined here, as well as model calculations (*24*), suggested that this level of uncertainty did not affect the essential conclusions of our study. Our laboratory now uses connection fittings that are much less prone to leaks.

Certain hopanes exhibited slight losses in the surf zone. The C_{30}−C_{35} hopanes are often assumed conserved over years of weathering (*12*, *32*), although hopane degradation can occur within weeks under certain conditions (*33*). Known hopane degradation pathways are believed to affect preferentially different members of the C_{30}−C_{35} hopanes (*33*, *34*).

Changes in relative abundances within this family should indicate degradation of one or more members; therefore we evaluated the abundance of each $C_{31}-C_{35}$ hopane normalized to C_{30} hopane across all samples (see Supporting Information). Relative to C_{30} hopane, the abundances of all $C_{31}-C_{35}$ hopanes remained constant to within 2−3% in the dry zone. Both the early (days 16, 33, 60) and late (days 86, 114) weathering segments of the dry zone series exhibited the same levels of variability for each hopane, hence we concluded that observed deviations reflected limits of measurement precision. By contrast, the surf zone samples displayed systematic losses of the heavier hopanes starting after day 60. In the late summer surf zone samples (days 86A−C, 114), C_{32} hopane showed 5.0 ± 1.5% loss, and C_{33} hopane showed 8.2 ± 1.3% loss, relative to the original cargo oil. The $C_{34}-C_{35}$ hopane set showed 10.3 ± 1.5% loss on day 86 and 16.3 ± 1.6% loss on day 114. Since the 3 day 86 surf zone samples were believed compromised by a small column fitting leak (explained above), this artifact could contribute to the apparent loss trends in late summer surf zone samples. Taken together, these observations indicate that significant C_{30} hopane losses were very unlikely to have occurred in the dry zone, and minor C_{30} hopane losses may have occurred in the surf zone. Overall, we concluded that C_{30} hopane was a reasonable internal marker for this study.

Having established quantitative mass loss trends resulting from evaporation and dissolution, we identified hydrocarbon degradation processes as additional mass losses that are superimposed onto mass transfer signatures. By inspection of each MLT row and column, we roughly estimated mass losses due to evaporation and dissolution for the corresponding sections in the GC×GC chromatogram. Then, assuming that different weathering processes affect compounds independently (*24*), individual compound mass loss due to degradation was determined as the difference between observed peak volume change and the estimated loss resulting from evaporation plus dissolution. While a broad evaluation of hydrocarbon degradation in Nyes Neck samples is beyond the scope of the current paper, we briefly discuss two examples of such an analysis below. Note that in our companion manuscript (*24*), an alternative mass apportionment approach is developed and applied to the comprehensive hydrocarbon mixture, based on mass transfer calculations.

The *n*-alkanes were mostly depleted by day 114, primarily due to biodegradation. Consistent with Slater et al.'s study (*35*) of this same spill site, *n*-alkanes showed significant mass losses not explainable by evaporation starting at day 33, indicating biodegradation (see Supporting Information). For aggregate *n*-alkane mass, we estimated evaporation loss rates of 0.0016 ± 0.0003 day^{-1} (dry zone) and 0.0007 ± 0.0004 day^{-1} (surf zone) and biodegradation loss rates of 0.009 ± 0.002 day^{-1} (dry zone) and 0.008 ± 0.001 day^{-1} (surf zone). Note that these rates reflect only early weathering kinetics, since the evaporation rate of aggregate *n*-alkane mass is not expected to exhibit first-order kinetics (*24*). On inspection of the chemical property map (Figure 1a), the aliphatic hydrocarbon fractions occupy the bottom row (i.e., lowest solubility) of the MLT (Figure 2d). In many samples, this MLT row was depleted faster than nearby rows, suggesting that an additional mass removal process was superimposed onto the evaporation front (Figure 3). Biodegradation preferentially affected *n*-alkanes smaller than C_{27}; this is consistent with the previous observation that biodegradative attack favors decreased size for saturated hydrocarbons (*7*).

We suspect that photodegradation became significant for some compounds after the first 2 months of *Bouchard 120* weathering. Photoreactions preferentially target PAHs with increasing alkyl substitution and increasing size (*8*, *32*), and these compound groups were not affected until mid summer. For example, detectable losses of C_2-pyrenes were superimposed onto dissolution and evaporation signatures in many of the day 60 and day 86 samples (Figures 2d and 3), suggesting photodegradation. Day 114 samples were sufficiently severely weathered that these processes were more difficult to differentiate for the C_2-pyrenes. In both day 114 samples, a broad range of high molecular weight compounds showed significant depletion, suggesting losses due to biodegradation and/or photodegradation.

Implications for the Study of Oil Weathering. The approaches described here complement existing analysis methods and enable new insights into oil weathering. Because the physical properties of analyzed solutes are estimated directly from GC×GC retention times, exact knowledge of their compound structures is not necessary, assuming they are hydrocarbons. As a consequence, mass loss tables reflect mass removal rates of thousands of different compounds. By comparison, conventional ratios reflect information about only a handful of compounds. Our approach allowed robust quantitative constraints on evaporation and dissolution across the compositional space of a weathered oil. This enabled a rigorous evaluation of mass transfer models in a field context (the Part 2 companion to this paper). Improved accounting of mass transfers should advance our understanding of biodegradation and phototransformation in the field and also improve estimates of hydrocarbon concentrations in the water column. Hence the methods described here should lead to improved assessments of wildlife exposures to hydrocarbons after oil spills.

Acknowledgments

We gratefully acknowledge the constructive comments of Dr. Roger Prince and three anonymous reviewers. This work was supported by the NSF (MPS-DRF-CHE-0502600 and IIS-0430835), DOE (DEFG02-06ER15775), and ONR (N00014-04-01-0029).

Supporting Information Available

Summary of the custom peak integration algorithm; $C_{31}-C_{35}$ 17α,21β(H) hopane concentrations, normalized to C_{30} 17α,-21β(H) hopane; $C_{11}-C_{34}$ *n*-alkane mass relative to the original *Bouchard 120* oil, normalized to C_{30} 17α,21β(H) hopane; and aggregate $C_{11}-C_{34}$ *n*-alkane mass relative to the original *Bouchard 120* oil for dry zone and surf zone. This material is available free of charge via the Internet at http://pubs.acs.org.

Literature Cited

(1) National Research Council. *Oil in the Sea III. Inputs, Fates and Effects*; National Academy of Sciences: Washington, DC, 2003.

(2) Mackay, D.; Matsugu, R. S. Evaporation rates of liquid hydrocarbon spills on land and water. *Can. J. Chem. Eng.* **1973**, *51*, 434−439.

(3) Blumer, M.; Ehrhardt, M.; Jones, J. H. The environmental fate of stranded crude oil. *Deep-Sea Res.* **1973**, *20*, 239−259.

(4) Harrison, W.; Winnik, M. A.; Kwong, P. T. Y.; Mackay, D. Crude oil spills. Disappearance of aromatics and aliphatic components from small sea-surface slicks. *Environ. Sci. Technol.* **1975**, *9*, 231−234.

(5) Schwarzenbach, R. P.; Gschwend, P. M.; Imboden, D. M. *Environmental Organic Chemistry*, 2nd ed.; John Wiley & Sons: New York, 2003.

(6) Larson, R. A.; Hunt, L. L.; Blankenship, D. W. Formation of toxic products from a #2 fuel oil by photooxidation. *Environ. Sci. Technol.* **1977**, *11*, 492−496.

(7) Volkman, J. K.; Alexander, R.; Kagi, R. I.; Rowland, S. J.; Sheppard, P. N. Biodegradation of aromatic hydrocarbons in crude oils from the Barrow sub-basin of western Australia. *Org. Geochem.* **1984**, *6*, 619−632.

(8) Garrett, R. M.; Pickering, I. J.; Haith, C. E.; Prince, R. C. Photooxidation of crude oils. *Environ. Sci. Technol.* **1998**, *32*, 3719−3723.

(9) French, D. P. In *Twenty-first Arctic and Marine Oil spill Program (AMOP) Technical Seminar*, June 10−12, 1998, West Edmonton, Alberta, Canada, 1998.

(10) Lee, R. F.; Page, D. S. Petroleum hydrocarbons and their effects in subtidal regions after major oil spills. *Mar. Pollut. Bull.* **1997**, *34*, 928−940.

(11) Carls, M. G.; Rice, S. D.; Hose, J. E. Sensitivity of fish embryos to weathered crude oil: Part I. Low-level exposure during incubation causes malformations, genetic damage, and mortality in larval Pacific Herring (*Clupea pallasi*). *Environ. Toxicol. Chem.* **1999**, *18*, 481−493.

(12) Wang, Z.; Fingas, M. F. Development of oil hydrocarbon fingerprinting and identification techniques. *Mar. Pollut. Bull.* **2003**, *47*, 423−452.

(13) Douglas, G. S.; Bence, A. E.; Prince, R. C.; McMillen, S. J.; Butler, E. L. Environmental stability of selected petroleum hydrocarbon source and weathering ratios. *Environ. Sci. Technol.* **1996**, *30*, 2332−2339.

(14) Boehm, P. D.; Flest, D. L.; Mackay, D.; Paterson, S. Physical-chemical weathering of petroleum hydrocarbons from the Ixtoc I blowout: Chemical measurements and a weathering model. *Environ. Sci. Technol.* **1982**, *16*, 498−505.

(15) Bence, A. E.; Kvenvolden, K. A.; Kennicutt, M. C. Organic geochemistry applied to environmental assessments of Prince William Sound, Alaska, after the *Exxon Valdez* oil spill - a review. *Org. Geochem.* **1996**, *24*, 7−42.

(16) Wang, Z.; Fingas, M. F. Study of the effects of weathering on the chemical composition of a light crude oil using GC/MS GC/FID. *J. Microcolumn Sep.* **1995**, *7*, 617−639.

(17) Wang, Z.; Fingas, M. F. Forensic fingerprinting of biomarkers for oil spill characterization and source identification. *Environ. Forens.* **2006**, *7*, 105−146.

(18) Liu, Z. Y.; Phillips, J. B. Comprehensive 2-Dimensional Gas-Chromatography using an on-column thermal modulator interface. *J. Chromatogr. Sci.* **1991**, *29*, 227−231.

(19) Frysinger, G. S.; Gaines, R. B.; Xu, L.; Reddy, C. M. Resolving the unresolved complex mixture in petroleum-contaminated sediments. *Environ. Sci. Technol.* **2003**, *37*, 1653−1662.

(20) Booth, A. M.; Sutton, P. A.; Lewis, C. A.; Lewis, A. C.; Scarlett, A.; Chau, W.; Widdows, J.; Rowland, S. J. Unresolved complex mixtures of aromatic hydrocarbons: Thousands of overlooked persistent, bioaccumulative, and toxic contaminants in mussels. *Environ. Sci. Technol.* **2007**, *41*, 457−464.

(21) Frysinger, G. S.; Gaines, R. B. Separation and identification of petroleum biomarkers by comprehensive two-dimensional gas chromatography. *J. Sep. Sci.* **2001**, *24*, 87−96.

(22) Arey, J. S.; Nelson, R. K.; Xu, L.; Reddy, C. M. Using comprehensive two-dimensional gas chromatography retention indices to estimate environmental partitioning properties for a complete set of diesel fuel hydrocarbons. *Anal. Chem.* **2005**, *77*, 7172−7182.

(23) Arey, J. S.; Nelson, R. K.; Xu, L.; Reddy, C. M. Using comprehensive two-dimensional gas chromatography retention indices to estimate environmental partitioning properties for a complete set of diesel fuel hydrocarbons, correction. *Anal. Chem.* **2007**, *79*, 4736.

(24) Arey, J. S.; Nelson, R. K.; Plata, D. L.; Reddy, C. M. Disentangling oil weathering using GC×GC. 2. Mass transfer calculations. *Environ. Sci. Technol.* **2007**, *41*, 5747−5755.

(25) Nelson, R. K.; Kile, B. M.; Plata, D. L.; Sylva, S. P.; Xu, L.; Reddy, C. M.; Gaines, R. B.; Frysinger, G. S.; Reichenbach, S. E. Tracking the weathering of an oil spill with comprehensive two-dimensional gas chromatography. *Environ. Forens.* **2006**, *7*, 33−44.

(26) Reichenbach, S. E.; Ni, M.; Zhang, D.; Ledford, E. B. Image background removal in comprehensive two-dimensional gas chromatography. *J. Chromatogr. A* **2003**, *985*, 47−56.

(27) Reichenbach, S. E.; Ni, M.; Kottapalli, V.; Visvanathan, A. Information technologies for comprehensive two-dimensional gas chromatography. *Chemom. Intell. Labt. Syst.* **2004**, *71*, 107−120.

(28) Prince, R. C.; Elmendorf, D. L.; Lute, J. R.; Hsu, C. S.; Halth, C. E.; Senius, J. D.; Dechert, G. J.; Douglas, G. S.; Butler, E. L. 17a-(H),21b(H)-hopane as a conserved internal marker for estimating the biodegradation of crude oil. *Environ. Sci. Technol.* **1994**, *28*, 142−145.

(29) Cline, P. V.; Delfino, J. J.; Rao, P. S. C. Partitioning of aromatic constituents into water from gasoline and other complex solvent mixtures. *Environ. Sci. Technol.* **1991**, *25*, 914−920.

(30) Bidleman, T. F. Estimation of vapor pressures for nonpolar organic compounds by capillary gas chromatography. *Anal. Chem.* **1984**, *56*, 2490−2496.

(31) Reddy, C. M.; Eglinton, T. I.; Hounshell, A.; White, H. K.; Xu, L.; Gaines, R. B.; Frysinger, G. S. The West Falmouth oil spill after thirty years: The persistence of petroleum hydrocarbons in marsh sediments. *Environ. Sci. Technol.* **2002**, *36*, 4754−4760.

(32) Prince, R. C.; Garrett, R. M.; Bare, R. E.; Grossman, M. J.; Townsend, T.; Suflita, J. M.; Lee, K.; Owens, E. H.; Sergy, G. A.; Braddock, J. F.; Lindstrom, J. E.; Lessard, R. R. The roles of photooxidation and biodegradation in long-term weathering of crude and heavy fuel oils. *Spill Sci. Technol. Bull.* **2003**, *8*, 145−156.

(33) Frontera-Suau, R.; Bost, F. D.; McDonald, T. J.; Morris, P. J. Aerobic biodegradation of hopanes and other biomarkers by crude oil-degrading enrichment cultures. *Environ. Sci. Technol.* **2002**, *36*, 4585−4592.

(34) Wang, Z.; Fingas, M. F.; Owens, E. H.; Sigouin, L.; Brown, C. E. Long-term fate and persistence of the spilled Metula oil in a marine salt marsh environment. Degradation of petroleum biomarkers. *J. Chromatogr. A* **2001**, *926*, 275−290.

(35) Slater, G. F.; Nelson, R. K.; Kile, B. M.; Reddy, C. M. Intrinsic bacterial biodegradation of petroleum contamination demonstrated *in situ* using natural abundance, molecular-level ^{14}C analysis. *Org. Geochem.* **2006**, *37*, 981−989.

(36) Wang, Z.; Fingas, M. F.; Sergy, G. A. Study of 22-year old *Arrow* oil samples using biomarker compounds by GC/MS. *Environ. Sci. Technol.* **1994**, *28*, 1733−1746.

(37) Wang, Z.; Fingas, M. F.; Sergy, G. A. Chemical characterization of crude oil residues from an arctic beach by GC/MS and GC/FID. *Environ. Sci. Technol.* **1995**, *29*, 2622−2631.

(38) Snape, I.; Harvey, P. M.; Ferguson, S. H.; Rayner, J. L.; Revill, A. T. Investigation of evaporation and biodegradation of fuel spills in Antarctica I. A chemical approach using GC-FID. *Chemosphere* **2005**, *61*, 1485−1494.

(39) Wang, Z.; Fingas, M. F.; Blenkinsopp, S.; Sergy, G. A.; Landriault, M.; Sigouin, L.; Foght, J.; Semple, K.; Westlake, D. W. S. Comparison of oil composition changes due to biodegradation and physical weathering in diffferent oils. *J. Chromatogr. A* **1998**, *809*, 89−107.

(40) Wang, Z.; Fingas, M. F.; Blenkinsopp, S.; Sergy, G. A.; Landriault, M.; Sigouin, L.; Lambert, P. Study of the 25-year-old Nipisi oil spill: Persistence of oil residues and comparisons between surface and subsurface sediments. *Environ. Sci. Technol.* **1998**, *32*, 2222−2232.

(41) Wang, Z.; Fingas, M. F. Differentiation of the source of spilled oil and monitoring of the oil weathering process using gas chromatography-mass spectrometry. *J. Chromatogr. A* **1995**, *712*, 321−343.

(42) Gundlach, E. R.; Boehm, P. D.; Marchand, M.; Atlas, R. M.; Ward, D. M.; Wolfe, D. A. The fate of *Amoco Cadiz* oil. *Science* **1983**, *221*, 122−129.

(43) Sauer, T. C.; Michel, J.; Hayes, M. O.; Aurand, D. V. Hydrocarbon characterization and weathering of oiled intertidal sediments along the Saudi Arabian coast two years after the Gulf War oil spill. *Environ. Int.* **1998**, *24*, 43−60.

(44) Ezra, S.; Feinstein, S.; Ithamar, P.; Bauman, D.; Miloslavsky, I. Weathering of fuel oil spill on the east Mediterranean coast, Ashdod, Israel. *Org. Geochem.* **2000**, *31*, 1733−1741.

(45) Lee, K.; Prince, R. C.; Greer, C. W.; Doe, K. G.; Wilson, J. E. H.; Cobanli, S. E.; Wohlgeschaffen, G. D.; Alroumi, D.; King, T.; Tremblay, G. H. Composition and toxicity of residual Bunker C fuel in intertidal sediments after 30 years. *Spill Sci. Technol. Bull.* **2003**, *8*, 187−199.

(46) Douglas, G. S.; Owens, E. H.; Hardenstein, J.; Prince, R. C. The OSSA II pipeline oil spill: the character and weathering of the spilled oil. *Spill Sci. Technol. Bull.* **2002**, *7*, 135−148.

(47) Jezequel, R.; Menot, L.; Merlin, F.-X.; Prince, R. C. Natural cleanup of heavy fuel oil on rocks: an in situ experiment. *Mar. Pollut. Bull.* **2003**, *46*, 983−990.

(48) Sauer, T. C.; Brown, J. S.; Boehm, P. D.; Aurand, D. V.; Michel, J.; Hayes, M. O. Hydrocarbon source identification and weathering characterization of intertidal and subtidal sediments along the Saudi Arabian coast after the Gulf War oil spill. *Mar. Pollut. Bull.* **1993**, *27*, 117−134.

(49) Teal, J. M.; Farrington, J. W.; Burns, K. A.; Stegeman, J. J.; Tripp, B. W.; Woodin, B.; Phinney, C. The West Falmouth oil spill after 20 years: Fate of fuel oil compounds and effects on animals. *Mar. Pollut. Bull.* **1992**, *24*, 607−614.

(50) Michel, J.; Hayes, M. O. Weathering patterns of oil residues eight years after the *Exxon Valdez* oil spill. *Mar. Pollut. Bull.* **1999**, *38*, 855−863.

(51) Carls, M. G.; Babcock, M. M.; Harris, P. M.; Irvine, G. V.; Cusick, J. A.; Rice, S. D. Persistence of oiling in mussel beds after the *Exxon Valdez* oil spill. *Mar. Environ. Res.* **2001**, *51*, 167−190.

Received for review January 2, 2007. Revised manuscript received April 24, 2007. Accepted June 3, 2007.

ES070005X